Supplementary Materials

Diazines at graphene: adsorption, structural variances and electronic states

O. I. Grinevich,[a] V. V. Volkov,[b] A. K. Buryak[a,*]

[a]*A. N. Frumkin Institute of Physical Chemistry and Electrochemistry, Russian Academy of Sciences, 31 Leninsky Prospect, Moscow, GSP-1, 119071, Russian Federation*
[b]*Bereozovaya 2a, Konstantinivo, Moscow Region, 140207, Russian Federation*

Uniform surface limit by Kiselev [A. V. Kiselev. Intermolecular interactions in adsorption and chromatography. Moscow, High School, 1986]

The discussion of the second derivative of the potential energy stems from the theory of ideal adsorbed state. It is important to question applicability of the limit, but the universal law for gas adsorption does exist as the ideal limit is observed experimentally, when pressure approaches zero. Articulating adsorption, this corresponds to the Henry's Law according to the choice of a thermodynamic standard state.

Following this, thermodynamics of adsorption concerns accounting the relation of Henry's constant, K_1, as a macroscopic characteristic, with potential energy on intermolecular interaction, which depends on the structure of both, the adsorbate molecule and of the adsorbent. To manage the task, we need to adopt molecular-statistical theory of adsorption to express K_1 in dependence on temperature.

The general molecular-statistical expression for the chemical potential of the adsorbate in the gas phase, μ^g, and when adsorbed, μ,are:

$$\mu^g = -kT\,ln(Q^g/N^g)$$

$$\mu = -kT\,ln(Q/N)$$

where Q^g and Q are the canonical sums over states, while N^g and N are the numbers of molecules.

When equilibrium, $\mu^g = \mu$, we receive

$$\frac{N - N^g}{N^g} = \frac{Q - Q^g}{Q^g} \quad \text{or} \quad \frac{A(N - N^g)/A}{V(N^g/V)} = \frac{Q - Q^g}{Q^g}$$

where V and A are the volume of the gas phase and area of adsorption, respectively. Here, $(N - N^g)/A = \Gamma$ and $N^g/V = c$ represent Gibbs' adsorption and adsorbate concentration in the gas phase, respectively.

Next, to obtain a molecular-statistical expression for Henry's constant, let's pay attention to the fact that that, when $\Gamma \to 0$ and e $c \to 0$, one can neglect the interaction of adsorbate molecules with each other as in the gas phase, and in the adsorbed state. To distinguish this simple case, we adopt subscript 1

$$\lim_{\Gamma \to 0, c \to 0} \left(\frac{\Gamma}{c}\right) = K_1 = \frac{V}{A}\left(\frac{Q_1 - Q_1^g}{Q_1^g}\right) = \frac{V}{A}\left(\frac{Q_1}{Q_1^g} - 1\right)$$

Here, Q_1 and Q_1^g are the sums over states for non-interacting molecules.

In the case of relatively weak physical adsorption on an inert non-porous non-specific adsorbent with a homogeneous flat surface, it can be assumed that intramolecular degrees of freedom of quasi-rigid molecules (which do not possess an internal rotation and retain their configuration during adsorption) do not change. Accordingly, the corresponding terms in Q_1 and Q_1^g would be removed.

In the classical approximation, sums over states are expressed in terms of the corresponding configuration integrals

$$Q_1^{clas} = \frac{1}{\sigma h} \int \dots \int \exp\left[-H(kT)\right] dp_1 \dots dp_s dq_1 \dots . dq_s \qquad (1)$$

Here, *h* is the Planck constant, σ – number of symmetries, *s* – number of degrees of freedom, H is the Hamiltonian to account kinetic and potential energies, *p* and *q* are generalized impulses and coordinates.

In the case of a quasi-rigid molecules, when Γ → 0 and e c → 0, Hamiltonian accounts translation, vibration terms and potential energy of the interaction of molecule with the surface:

$$H = E_{tr} + E_{rot} + U.$$

In the case of a quasi-rigid molecule like pyridazine, Φ does not only depend on the position of the centre of mass, but also on the Euler orientation angles.

Let us express sums for the kinetic terms in Eq. (1), according to the translation energy expressed via the molecular mass, M, and impulses for the centre of mass:

$$E_{tr} = p_x^2/2M + p_y^2/2M + p_z^2/2M$$

Accounting Poisson integral equality

$$\int_{-\infty}^{+\infty} e^{-ax^2} dx = (\pi/a)^{0.5}$$

We may receive for p_x:

$$\int_{-\infty}^{+\infty} Exp[-p_x^2/2MkT]\, dp_x = (2\pi MkT)^{0.5}$$

And consequently:

$$Q_{1,tr} = \frac{1}{h^3} \int_{-\infty}^{+\infty} Exp[-E_{tr}/kT]\, dp_x dp_y dp_z = \frac{1}{h^3}(2\pi MkT)^{3/2}$$

Let us express sums for the rotation terms in Eq. (1), Fort voluminous molecules E_{rot} depend on the rotation momenta in the Euler space $\{p_\theta, p_\psi, p_\phi\}$. At the classic limit

$$Q_{1,rot} = \frac{1}{h^3}\int_{-\infty}^{+\infty} Exp[-E_{rot}/kT]\; dp_\theta dp_\psi dp_\phi$$

We may express rotation energy of a quasi-rigid molecule via principle components of inertia tensor

$$E_{rot} = \frac{1}{2}(I_A\omega_X^2 + I_B\omega_Y^2 + I_C\omega_Z^2)$$

where $\{\omega_X, \omega_Y, \omega_Z\}$ are the components of angular velocity of the coordinate system $\{X, Y, Z\}$ specific to the molecular frame and rotating in respect to the $\{x, y, z\}$ system characteristic to the adsorbent. To conduct integrations, we need to express angular velocities using Euler variables:

$$\begin{cases} \omega_X = Sin\psi\; Sin\theta\dfrac{d\varphi}{dt} + Cos\psi\dfrac{d\theta}{dt} \\ \omega_Y = Cos\psi\; Cos\theta\dfrac{d\varphi}{dt} + Sin\psi\dfrac{d\theta}{dt} \\ \omega_Z = Cos\theta\dfrac{d\varphi}{dt} + \dfrac{d\varphi}{dt} \end{cases}$$

Accordingly,

$$E_{rot} = \frac{1}{2I_A}\left[p_\theta Cos\psi - (p_\varphi - p_\psi Cos\theta)\frac{Sin\psi}{Sin\theta}\right]^2 + \frac{1}{2I_B}\left[p_\theta Sin\psi - (p_\varphi - p_\psi Cos\theta)\frac{Cos\psi}{Sin\theta}\right]^2 + \frac{1}{2I_C}[p_\varphi]^2$$

Let us adopt the inertia components' multipliers as new variable:

$$\begin{cases} u = p_\theta Cos\psi - (p_\varphi - p_\psi Cos\theta)\dfrac{Sin\psi}{Sin\theta} \\ v = p_\theta Sin\psi - (p_\varphi - p_\psi Cos\theta)\dfrac{Cos\psi}{Sin\theta} \\ \omega = p_\varphi \end{cases}$$

$$E_{rot} = \frac{1}{2I_A}u^2 + \frac{1}{2I_B}v^2 + \frac{1}{2I_C}\omega^2$$

Hence,

$$Q_{1,rot} = \frac{1}{h^3}\int Exp\left[-\left(\frac{u^2}{2I_AkT} + \frac{v^2}{2I_BkT} + \frac{\omega^2}{2I_CkT}\right)\right] du\; dv\; d\omega\; Sin\theta\; d\theta\; d\psi\; d\phi$$

Adopting the same form of Poisson integral:

$$Q_{1,rot} = \frac{1}{h^3}\,(2\pi I_AkT)^{1/2}(2\pi I_BkT)^{1/2}(2\pi I_CkT)^{1/2}\int Sin\theta\; d\theta\; d\psi\; d\phi$$

Having the integrals, we may return to Eq. (1):

$$Q_1^{clas} = \frac{1}{\sigma h^6}(2\pi MkT)^{3/2}(2\pi I_AkT)^{1/2}(2\pi I_BkT)^{1/2}(2\pi I_CkT)^{1/2}\int\frac{U(\theta,\psi,\phi,x,y,z)}{kT}Sin\theta\; d\theta\; d\psi\; d\phi dxdydz$$

Here, the potential energy of interaction depends on the stationary {*x,y,z*} coordinate system specific to the adsorbent and on the $\{\theta,\psi,\phi\}$ rotation angles of the orientations of the main axes of the molecule at the surface.

Using this, we may express Henry's constant

$$K_1 = \frac{V}{A}\left(\frac{Q_1 - Q_1^g}{Q_1^g}\right) = \frac{V\int\left(Exp\left[-\frac{U}{kT}\right]-1\right)Sin\theta\, d\theta\, d\psi\, d\phi dxdydz}{A\int Sin\theta\, d\theta\, d\psi\, d\phi dxdydz}$$

$$K_1 = \frac{1}{8\pi^2 A}\int\left(Exp\left[-\frac{U}{kT}\right]-1\right)Sin\theta\, d\theta\, d\psi\, d\phi dxdydz \qquad (2)$$

Let us now consider the case of a heterocycle at carbonaceous surface.

Our results of quantum dynamics and DFT studies suggest that such molecule tend to orient parallel to the surface. Theory predicts weak energy modulation (c.a. 5 kJ/mol) when the molecule would slide parallel to the surface while experiencing angular reorientations. This allows considering the model developed for a linear molecule, with its long axis oriented perpendicular to the surface. In the case of a heterocycle, the normal to the plane at the centre of the cycle would play the role analogous to that of the long axis of a linear molecule.

Due to the relatively high density of carbon atoms (at the basal face of graphite and graphene), and their small size, a mathematically homogeneous surface is a good approximation for adsorption on such materials. Consistently, with the results of our dynamics simulation, we may relax the dependence of the potential energy onto x, y, ϕ, and ψ. Also, when the normal to the heterocycle plane co-aligns with the z to the surface

$$K_1 = \frac{1}{2}\int\left(Exp\left[-\frac{U}{kT}\right]-1\right)dz$$

Expanding , potential energy to the second term

$$U = U_0 + \frac{1}{2}U_z''(z - z_0)^2$$

where U_0 and U_z'' are the value and the second derivative (corresponds to the curvature) in the minimum z = z_0, respectively.

$$K_1 = \left(\frac{\pi kT}{U_z''}\right)^{1/2} Exp\left[-\frac{U_0}{kT}\right]$$

The expressed here analytical derivations should enable a reader to elaborate own models to account possible incomplete orientation averaging when using Eq. (2).

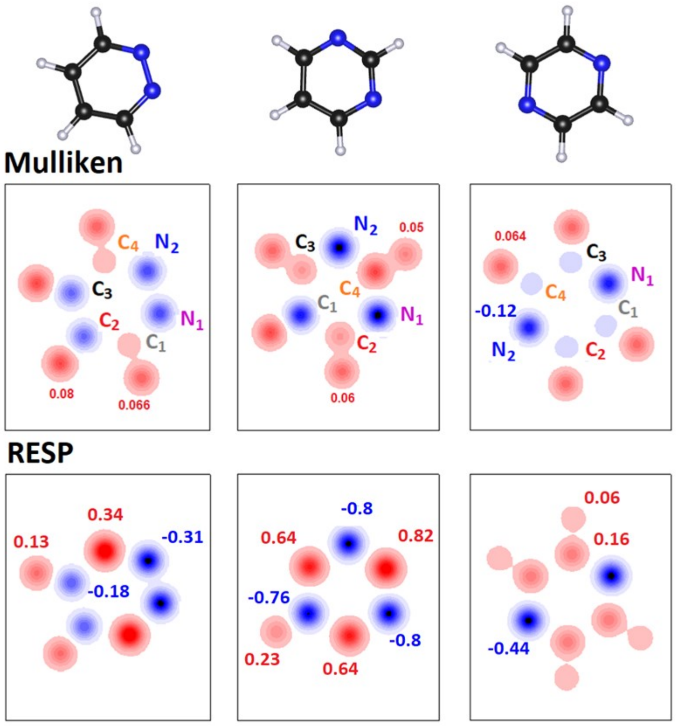

Fig. 1S. Structurally mapped Mulliken and restrained electrostatic potential (RESP) atomic charges [DOI: 10.1039/C4CP04638B] for pyridazine, pyrimidine and pyrazine computed using GWP/PB0 theory with MOLPOT pseudopotential basis.

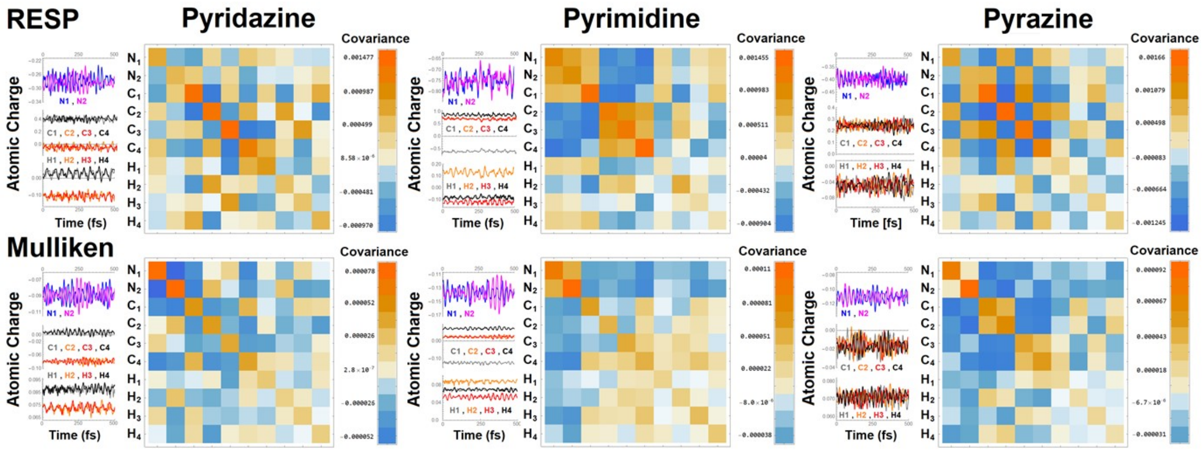

Fig. 2S. Changes of Mulliken and RESP atomic charges for pyridazine, pyrimidine and pyrazine on simulation time, and corresponding covariance matrices.

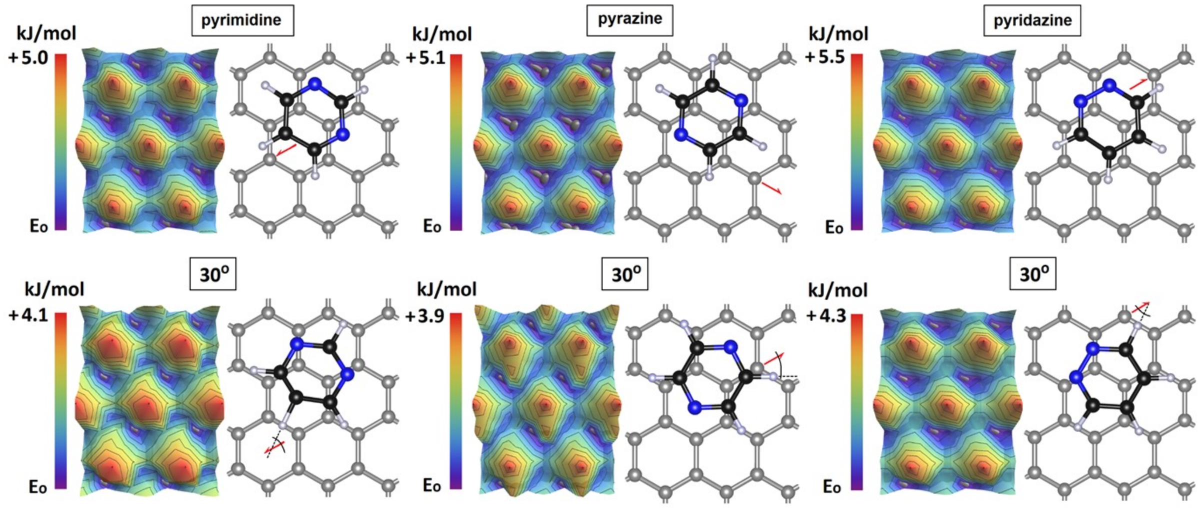

Fig. 3S. Energy in dependence on in-plane displacement of diazine six-membered heterocyclics and geometry of minimal energy. **Upper raw:** results for the arrangements, where a pair of CH bond of the heterocycles are parallel to the reference structural vectors (red), as shown. **Lower raw:** results for the arrangements, where each heterocycle was rotated in the XY plane about its centre, that their CH bonds (as indicated) would be under 30° in respect to the reference structural vectors (red), as shown. The data is computed using GWP/PB0 theory with MOLPOT pseudopotential basis.

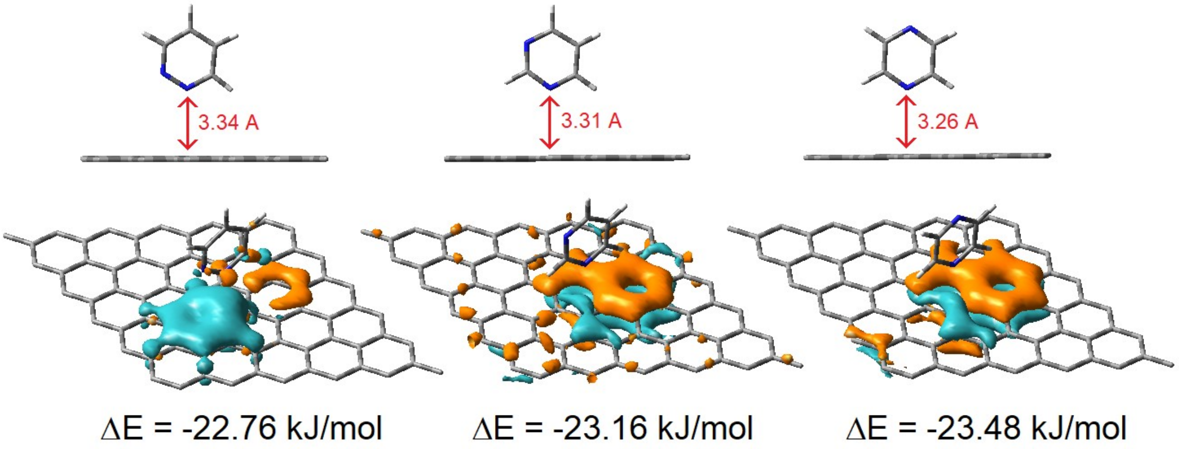

Fig. 4S. Electronic perturbations induced by diazine six-membered heterocyclics and energetic benefits of most the optimal associations under vertical orientations. The data is computed using GWP/PB0 theory, MOLPOT pseudopotential basis.

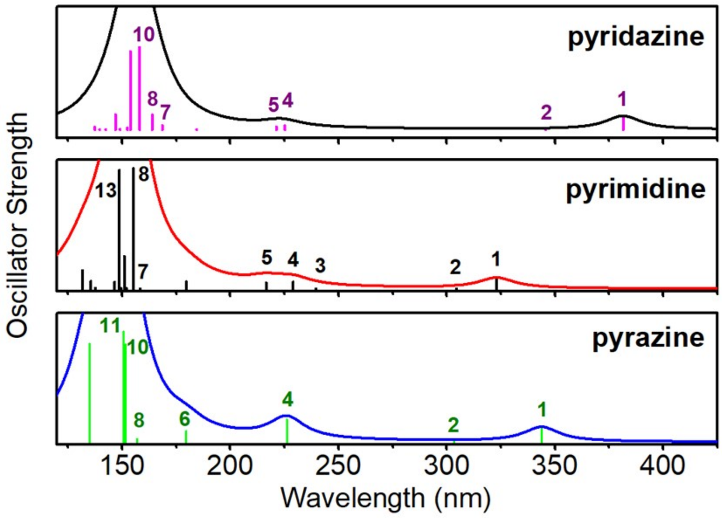

Fig. 5S. UV-VIS spectra for pyridazine, pyrimidine and pyrazine, as indicated, computed using TDDFPT: GWP/PB0, MOLPOT pseudopotential basis.

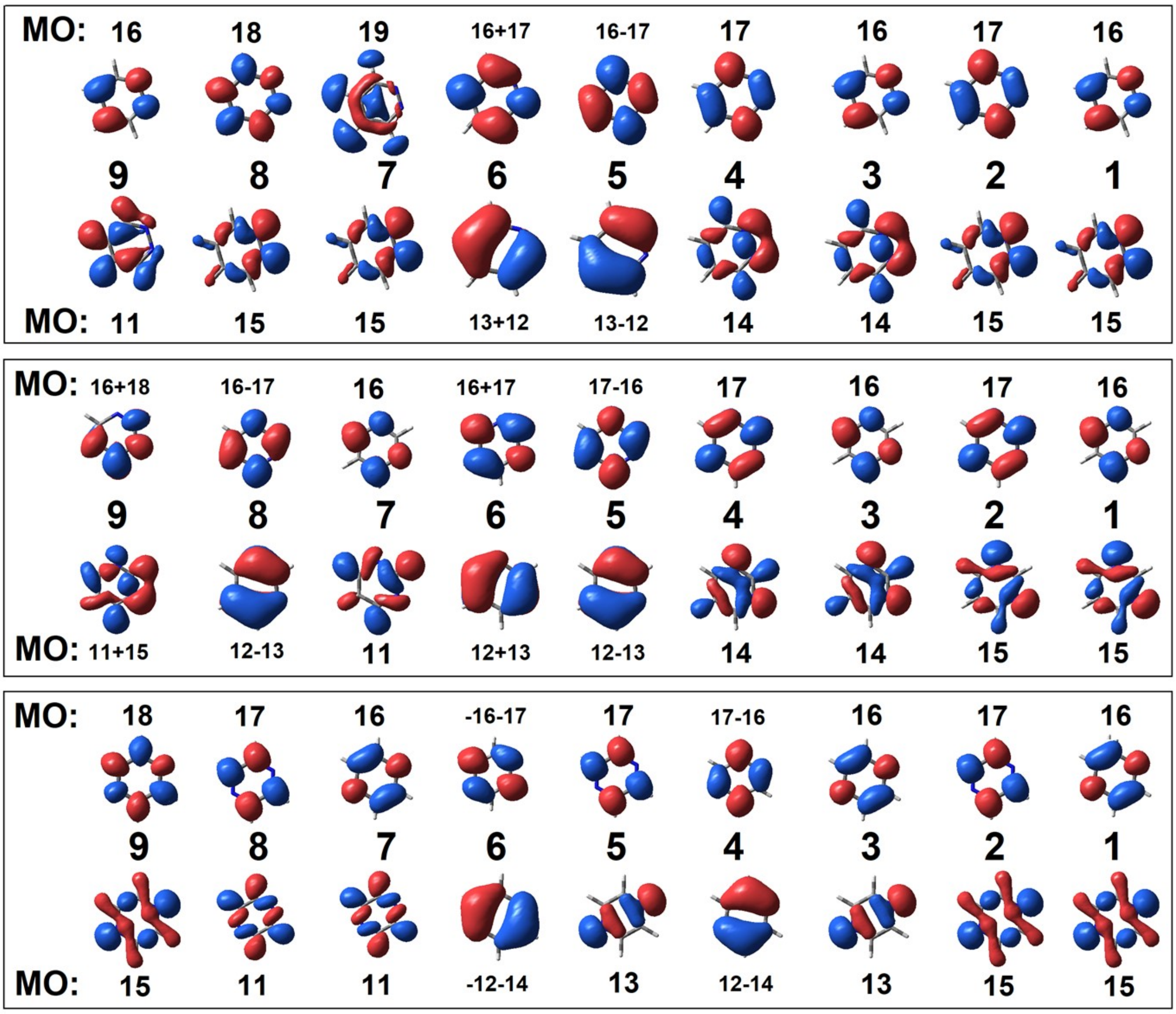

Fig. 6S. Computed electronic states providing electronic transitions as numbered computed for pyridazine (top), pyrimidine (middle) and pyrazine (bottom). In each panel, top and bottom numbers indicate Molecular Orbitals (MO) or their combination which contribute into the computed optical transitions. MO15 and MO16 are the HOMO and LUMO of the heterocycles.

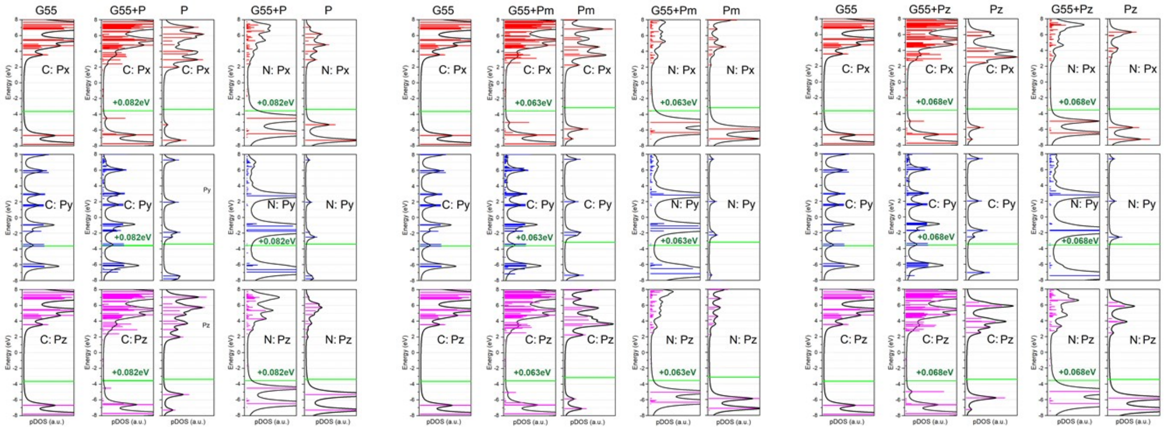

Fig. 7S. Projected density of states for G55 graphene systems, heterocycles alone (P: pyridazine, Pm: pyrimidine; Pz: pyrazine), and for the combinations of G55 with the heterocycles. Green lines indicate Fermi level, which are -3.6522 eV (G55), -3.57048 eV (G55+P), -3.58023 eV (G55+Pm), -3.58398 (G55+Pz), -3.38721 eV (P), -3.43132 eV (Pm), -3.16332 eV (Pz). The data is computed using GWP/PB0 with MOLPOT pseudopotential basis.

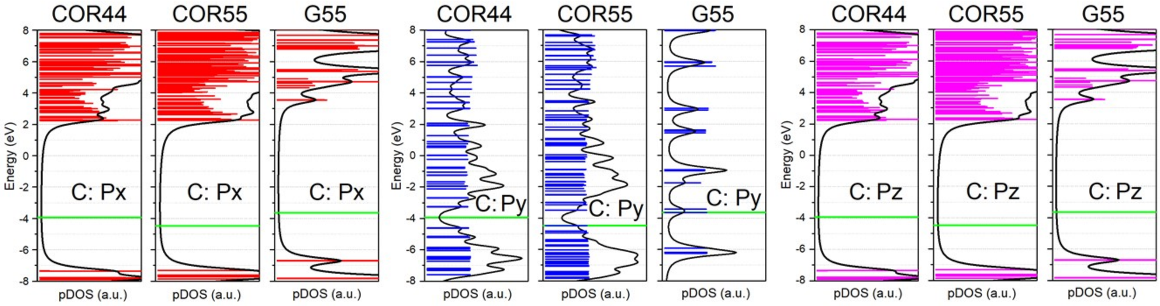

Fig. 8S. Projected density of states for coronenes COR44 and COR55, as well as, for G55 system. Green lines indicate Fermi level, which are -3.6522 eV (G55), -3.94042 eV (COR44), -4.48712eV (COR55). The data is computed using GWP/PB0 theory with MOLPOT pseudopotential basis.

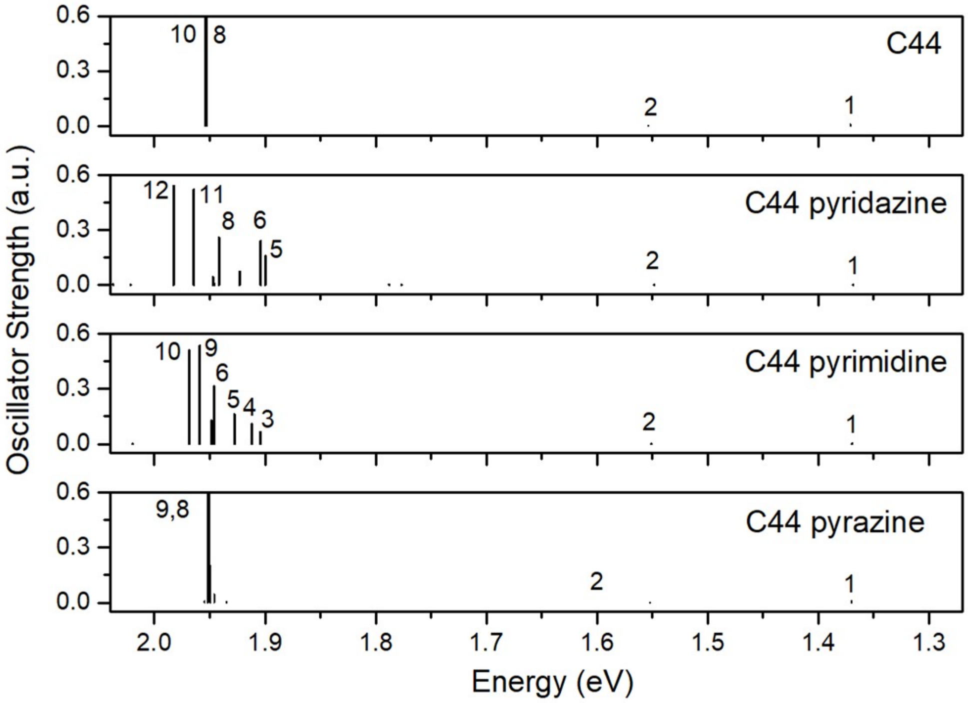

Fig. 9S. TDDFPT results for UV-VIS transitions computed for coronene C44, pyridazine at C44, pyrimidine at C44, and pyrazine at C44, as indicated. The data is computed using GWP/PB0 with MOLPOT pseudopotential basis.

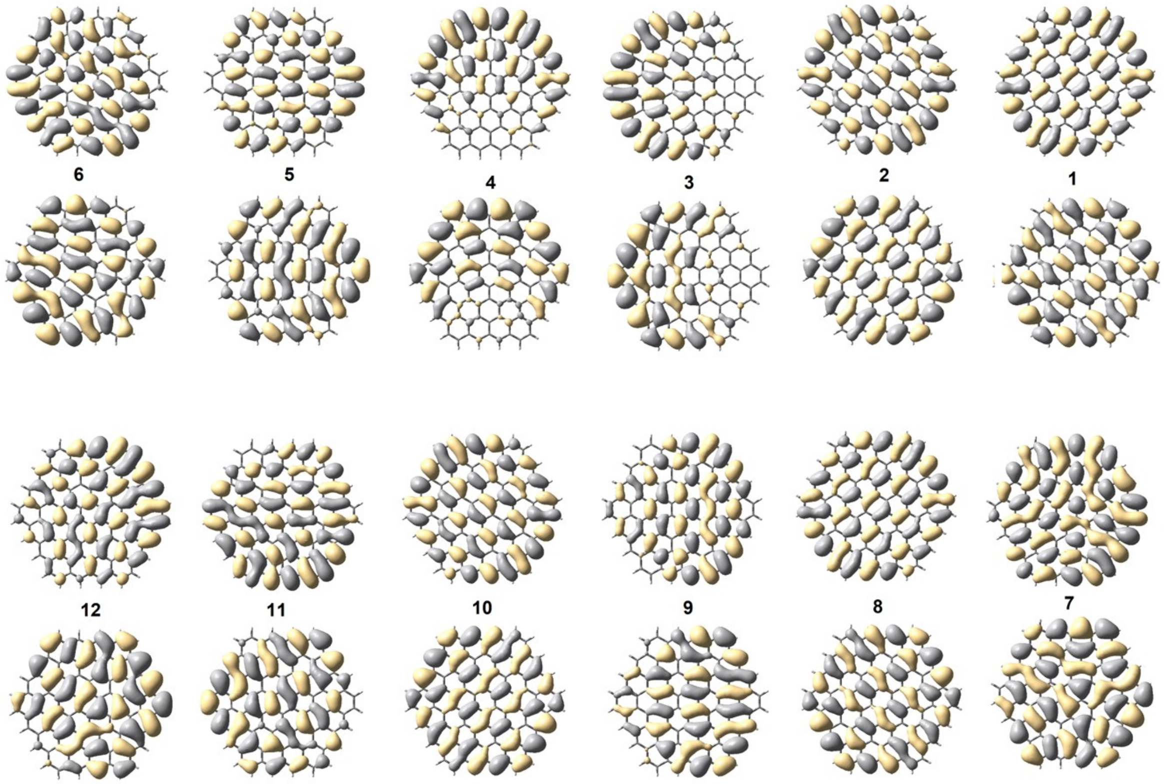

Fig. 10S. Electronic states for coronene C44 to provide optical electronic transitions as numbered. The data is computed using TDDFPT: GWP/PB0, MOLPOT pseudopotential basis.

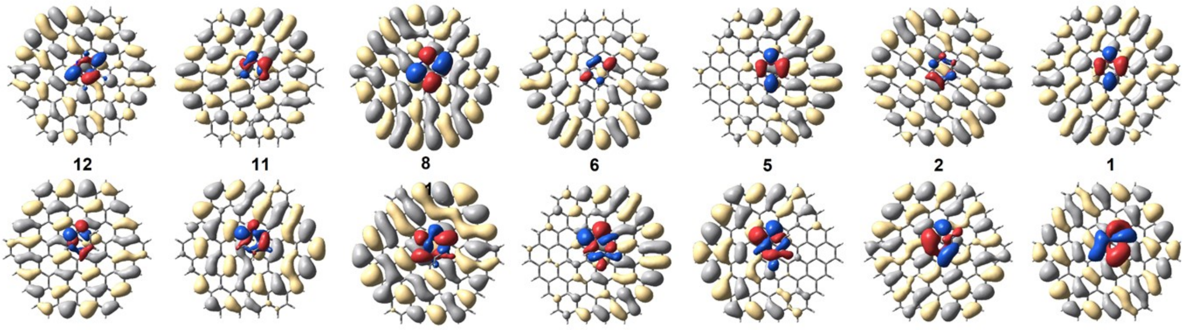

Fig. 11S. **E**lectronic states for pyridazine at C44 to provide optical electronic transitions, as numbered. We use blue-red and grey-yellow colors to contrast contributions of the heterocycles and graphene in the demonstrated mixed states. The data is computed using TDDFPT: GWP/PB0, MOLPOT pseudopotential basis.

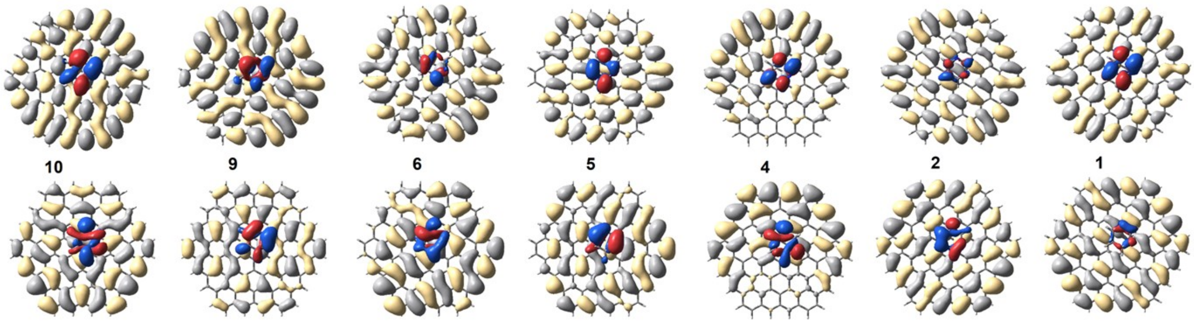

Fig. 12S. **E**lectronic states for pyrimidine at C44 to provide optical electronic transitions, as numbered. The data is computed using TDDFPT: GWP/PB0, MOLPOT pseudopotential basis.

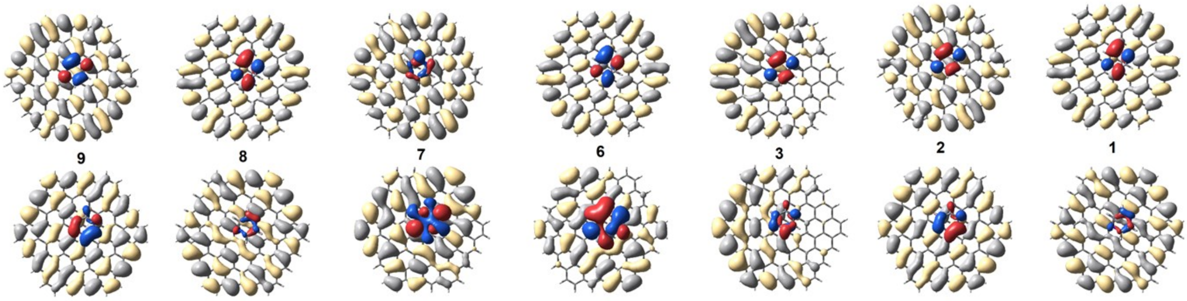

Fig. 13S. Electronic states for pyrazine at C44 to provide optical electronic transitions, as numbered. The data is computed using TDDFPT: GWP/PB0, MOLPOT pseudopotential basis.

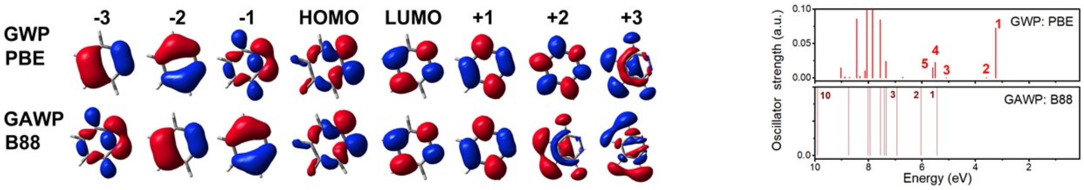

Fig. 14S. **Left:** canonical orbitals of pyridazine using GWP/PB0 theory with MOLPOT pseudopotential basis and GAWP/B88+Hartree-Fock exchange-correlation energy and long-range corrections theory with b3lyp basis, as specified. **Right:** transition frequencies for pyridazine using the two levels of theory. Since for the latter level of theory CP2K package does not allow fitting the wavefunctions under the TDDFPT protocol, the dashed lines in the panel of optical dispersion do not account oscillation strengths but serve as eye-guides indicating frequencies of computed resonances.

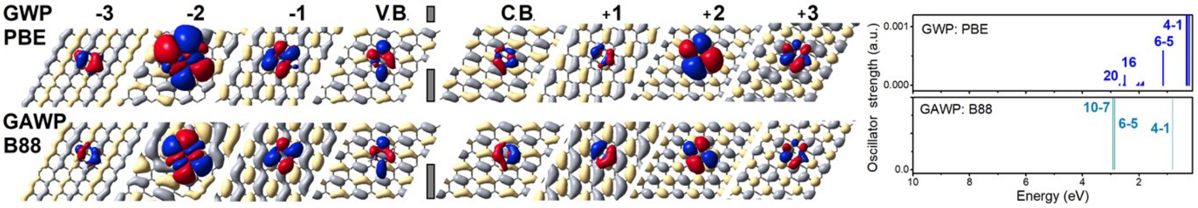

Fig. 15S. **Left:** canonical orbitals of pyridazine at graphene using GWP/PB0 theory with MOLPOT pseudopotential basis and GAWP/B88+Hartree-Fock exchange-correlation energy and long-range corrections theory with b3lyp basis, as indicated. **Right:** transition frequencies for pyridazine using the two levels of theory. Since for the latter level of theory CP2K package does not allow fitting the wavefunctions under the TDDFPT protocol, the dashed lines in the panel of optical dispersion do not account oscillation strengths but serve as eye-guides indicating frequencies of computed resonances.

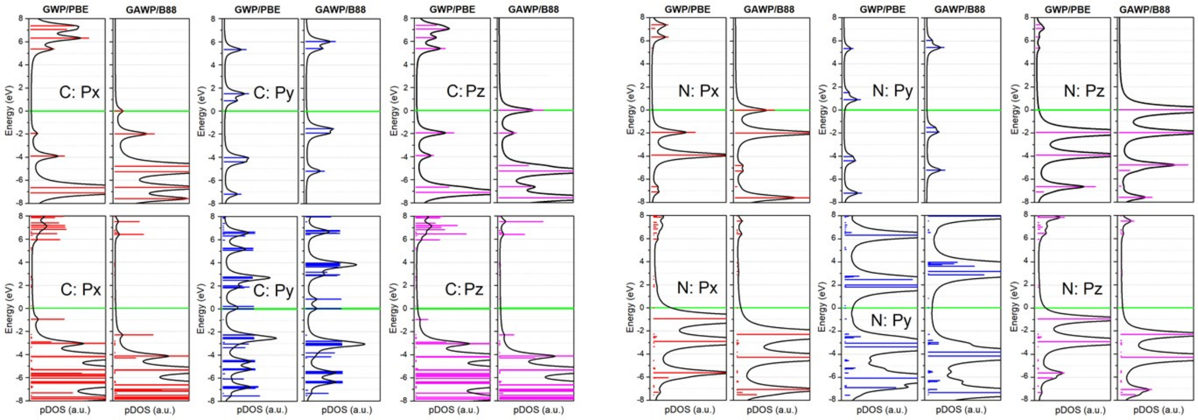

Fig. 16S. **Upper set:** projected densities of states computed for pyridazine. **Lower set:** projected densities of states computed for pyridazine at graphene. The data are computed using GWP/PB0 theory with MOLPOT pseudopotential basis and GAWP/B88+Hartree-Fock exchange-correlation energy and long-range corrections theory with b3lyp basis, as specified. For clarity of the comparisons, we subtract Fermi energies in both cases, as indicated by green lines.

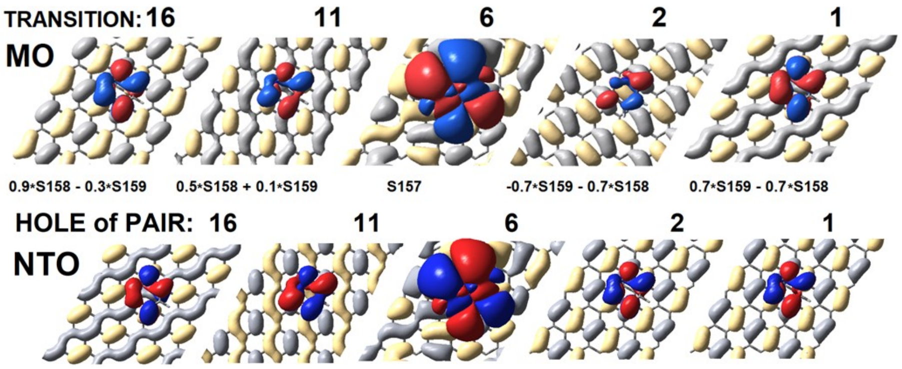

Fig. 17S. **Upper set:** departure states of the optical transitions (as indicated by numbers) for pyridazine at graphene according to canonical orbital presentation. Identifications under the images indicate weights and numbers of the canonical orbitals involved in the departure states. **Lower set:** natural transition orbital presentation. The data are computed using GWP/PB0 theory with MOLPOT pseudopotential basis.

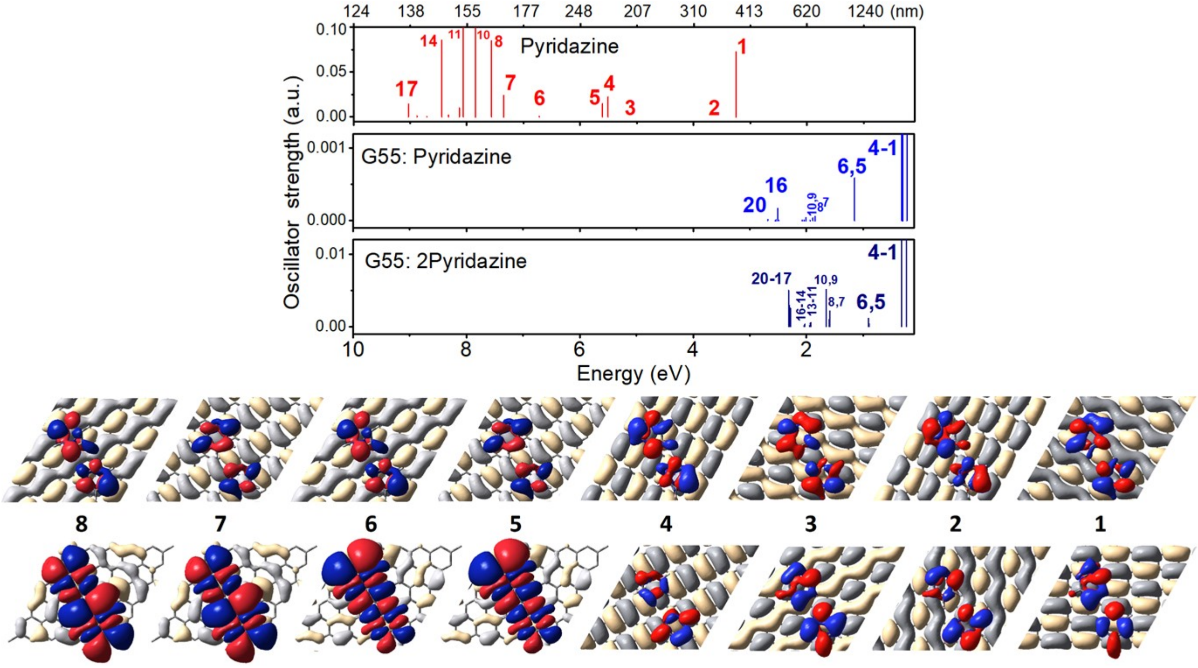

Fig. 18S. **Top:** Computed optical transitions for pyridazine in vacuum, single and paired pyridazine at graphene using TDDFPT protocol and GWP/PB0 theory with MOLPOT pseudopotential basis. **Bottom:** canonical orbitals of pyridazine at graphene to dominate the eight red-edge optical transitions, as indicated.